Обзор ArXiv/astro-ph, 20-30 мая 2019 года

От Сильченко О.К.

ArXiv: 1905.08818

Spatially-resolved stellar populations and kinematics with KCWI: probing the assembly history of the massive early-type galaxy NGC 1407

Anna Ferré-Mateu,[1,2] Duncan A. Forbes,[2] Richard M. McDermid,[3] Aaron J. Romanowsky,[4,5] and Jean P. Brodie[5]

[1] *Institut de Ciencies del Cosmos (ICCUB), Universitat de Barcelona (IEEC-UB), E02028 Barcelona, Spain*
[2] *Centre for Astrophysics & Supercomputing, Swinburne University of Technology, Hawthorn VIC 3122, Australia*
[3] *Department of Physics and Astronomy, Macquarie University, Sydney NSW 2109, Australia*
[4] *Department of Physics & Astronomy, San José State University, San Jose, CA 95192, USA*
[5] *University of California Observatories, 1156 High St., Santa Cruz, CA 95064, USA*

ABSTRACT

Using the newly commissioned KCWI instrument on the Keck-II telescope, we analyse the stellar kinematics and stellar populations of the well-studied massive early-type galaxy (ETG) NGC 1407. We obtained high signal-to-noise integral-field-spectra for a central and an outer (around one effective radius towards the south-east direction) pointing with integration times of just 600s and 2400s, respectively. We confirm the presence of a kinematically distinct core also revealed by VLT/MUSE data of the central regions. While NGC 1407 was previously found to have stellar populations characteristic of massive ETGs (with radially constant old ages and high alpha-enhancements), it was claimed to show peculiar super-solar metallicity peaks at large radius that deviated from an otherwise strong negative metallicity gradient, which is hard to reconcile within a 'two-phase' formation scenario. Our outer pointing confirms the near-uniform old ages and the presence of a steep metallicity gradient, but with no evidence for anomalously high metallicity values at large galactocentric radii. We find a rising outer velocity dispersion profile and high values of the 4th-order kinematic moment – an indicator of possible anisotropy. This coincides with the reported transition from a bottom-heavy to a Salpeter initial mass function, which may indicate that we are probing the transition region from the 'in-situ' to the accreted phase. With short exposures, we have been able to derive robust stellar kinematics

Новый IFU на телескопе Keck

Recently, two new IFS instruments have been installed on the Keck (Keck Cosmic Web Imager, KCWI; Morrissey et al. 2018) and the VLT (Multi Unit Spectroscopic Explorer, MUSE; Bacon et al. 2010) telescopes. Both instruments are designed for high sensitivity over long (stacked) total integration, and therefore are ideally suited to open up new avenues of study in the halos of ETGs. MUSE operates with a larger and longer wavelength coverage (480-930 nm) than KCWI, which currently operates with bluer coverage (350-560 nm, though with a planned future upgrade path for a red channel covering 530-1050 nm). The bluer coverage of KCWI is, however, arguably better suited to the study of stellar populations which have more diagnostic lines at blue wavelengths, as well as taking advantage of lower background contributions from night sky emission. MUSE has the advantage of a larger field-of-view (1'×1', compared to the 33"×20" corresponding to the largest FOV of KCWI), though the finer spatial sampling of MUSE (0.2″ square spaxels vs. KCWI's 0.4″×1.4″ in its largest field mode) is not necessarily an advantage for studying the extended envelopes of nearby galaxies, which can cover arcminute scales.

2. NGC 1407

Located at the centre of the massive Eridanus group (Gould 1993), NGC 1407 is the brightest group galaxy, classified as an E0. Its stellar mass is $\log(M_*/M_\odot) \simeq 11.60$ (Forbes et al. 2017)) and its total halo mass is $\log(M_h/M_\odot) \simeq 13.2$ (Wasserman et al. 2018). Here we take the distance to NGC 1407 (26.8 Mpc) and its effective radius (R_e = 63.4") from P+14 to enable direct comparison.

The galaxy has been extensively studied both with classical long-slit spectroscopy and with IFS. It has a recession velocity of v_r=1779 km s^{-1} and shows a well defined kinematically distinct core (KDC). This was first reported in Spolaor et al. (2008a) using long-slit spectroscopy, although the data were not sufficient to determine if it was a true feature. Since then, its kinematics in the central parts have been followed up by Proctor et al. (2009); Rusli et al. (2013); Arnold et al. (2014) and Foster et al. (2016). More recently, a new attempt to measure the size ($r \sim 5$ arcsec or 0.6 kpc) and amplitude of the KDC was performed with MUSE by (J+18). While they quote an amplitude of ~ 10 km s^{-1}, this is lower than that Rusli et al. (2013). Because the MUSE data was more coarse and seeing-limited, no conclusive results were reached.

Два наведения

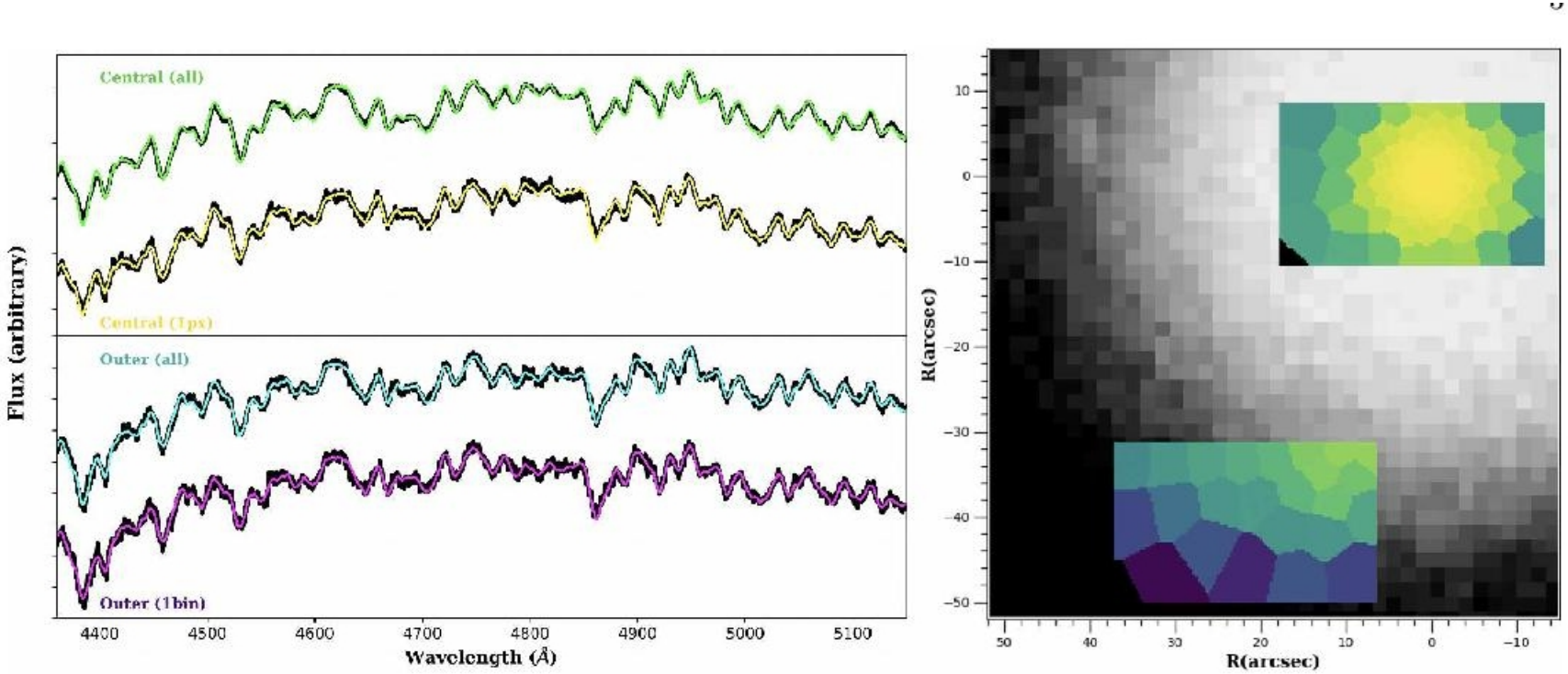

Figure 1. KCWI pointings of NGC 1407 and the resulting spectra: The two locations (central and outer) are shown as the tessellation map used in the analysis section, overlaid onto an DSS image of NGC 1407. North is up and East is left. The left panels show the corresponding spectra for the central (top) and outer (bottom) pointings and the resulting fitting from `pPXF`. Two apertures are shown in each case to illustrate the quality of the data. One corresponds to collapsing the entire datacube (green for the central, cyan for the outer) whereas the others correspond to the unbinned spectra for the center-most pixel (yellow) and the outermost bin of the outer pointing (magenta).

Сравнение кинематики с данными MUSE

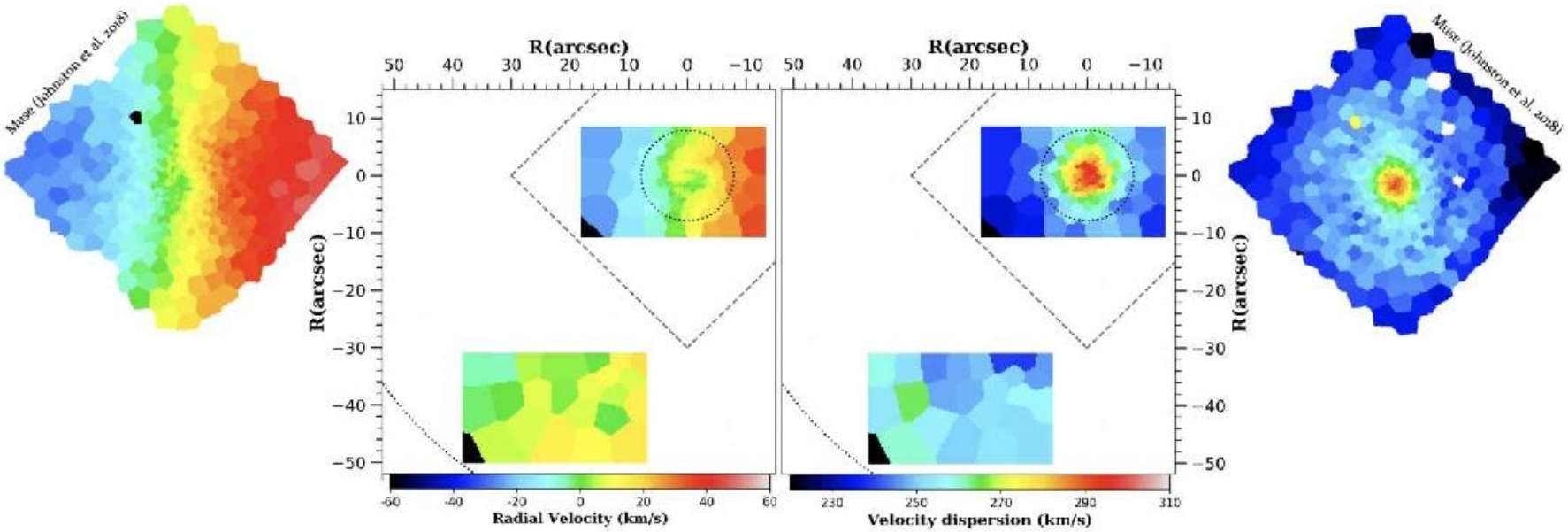

Figure 2. 2D stellar kinematic maps of NGC 1407: The KCWI low-order kinematics of NGC 1407 are shown, with the rotation velocity in the left panel and the velocity dispersion in the right panel. The small stamps on the sides (courtesy of E. Johnston) show the MUSE kinematic results from J+18 corresponding to the dashed diamond area in our panels, using the same color-scale. The dotted circles correspond to $R_e/8$ (smaller) and $1\,R_e$ (larger). The recovered kinematics in the central region are almost identical, including the presence of a KDC.

Дисперсия звезд растет наружу

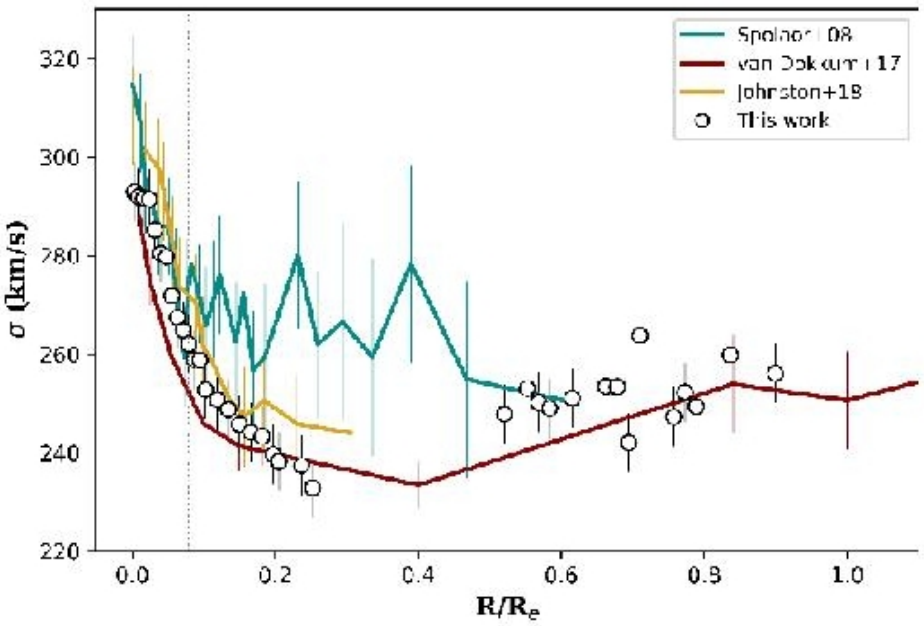

Figure 3. Radial velocity dispersion profile of NGC 1407: The 1D radial profile for the measured velocity dispersion from different literature works is shown. We find good agreement with literature studies, showing an increase outside of $\sim$0.3–0.4R_e. The dotted vertical line marks the size of the KDC from J+18.

Карта возрастов звезд

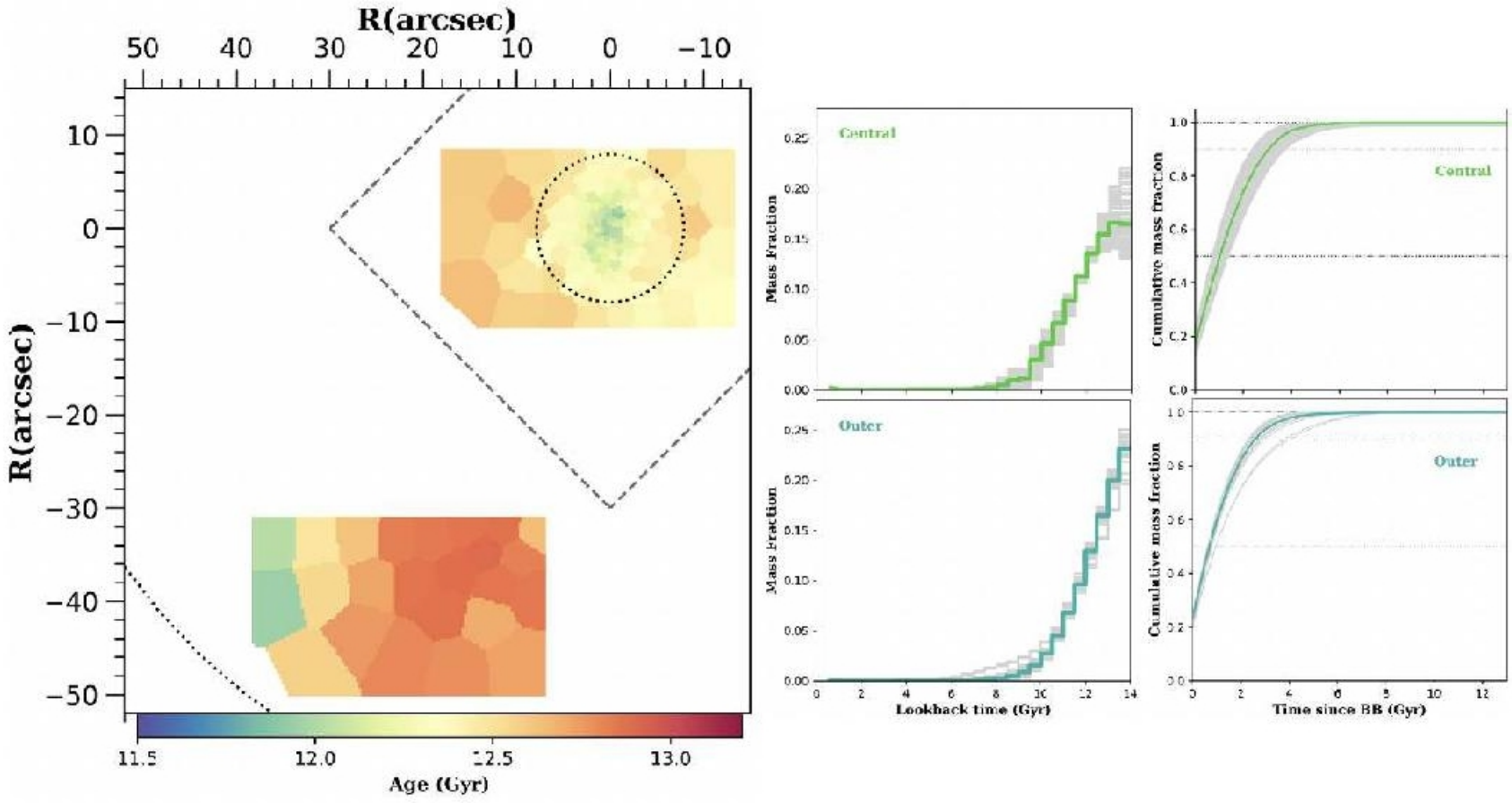

Figure 5. 2D map of the stellar ages in NGC 1407 and its SFH: *Left panel:* The 2D map shows that NGC 1407 is uniformly old, with a hint of slightly younger ages in the center. Note that there is a steep IMF out to $0.3R_e$, which corresponds to ∼30". *Right panels:* the SFHs and cumulative mass for each bin (grey) for the central (top) and outer (bottom) pointings. The solid green and cyan lines represent the averaged SFH and cumulative mass of the central and the outer pointings, respectively.

Карта металличностей звезд

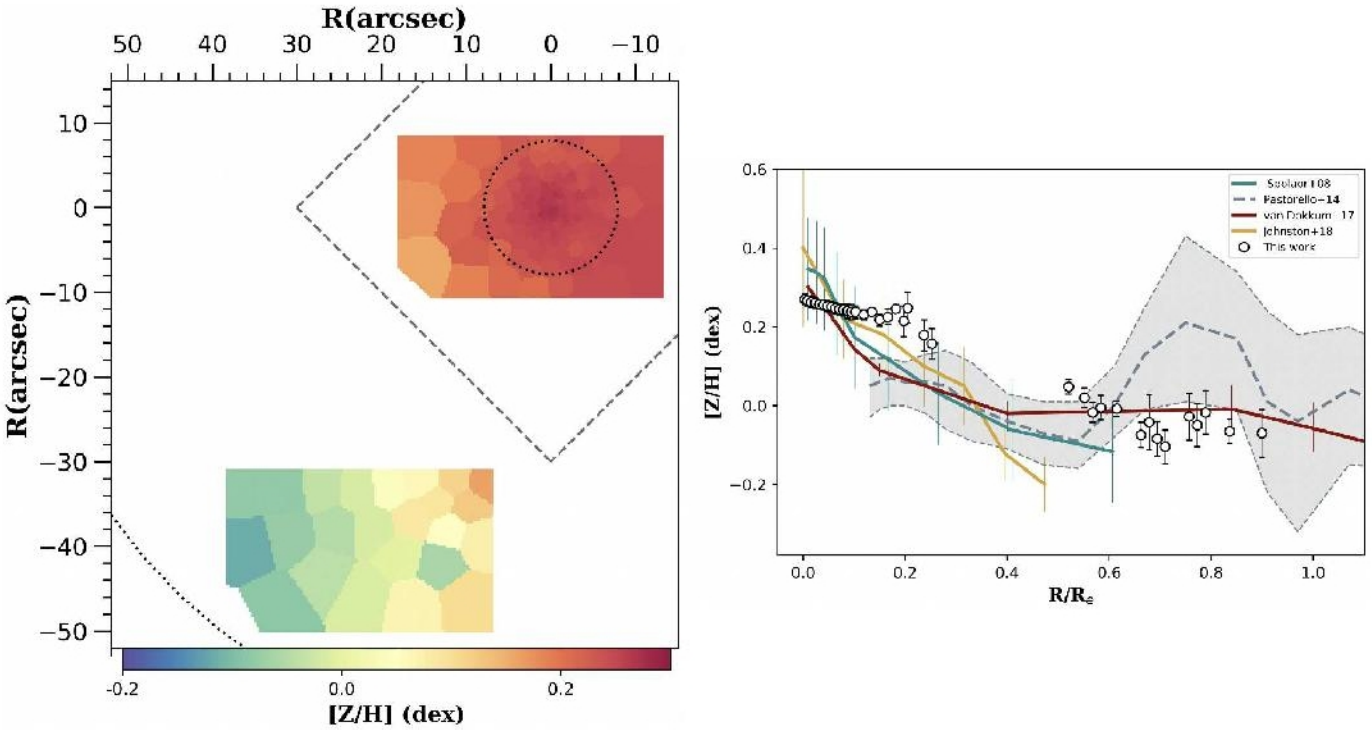

Figure 6. 2D map and radial profile of the metallicity in NGC 1407: *Left Panel:* the central and outer pointings reveal a strong radial negative metallicity gradient, with no evidence for anomalously high metallicities in the outer pointing. *Right panel:* metallicities from various literature studies are shown along with our KCWI measurements in two pointings (open circles).

although NGC 1407 is on average old (∼13 Gyr) the re- ETG. For example, the h_4 value of NGC 1407 is found

ArXiv: 1905.11356

The molecular gas content of shell galaxies ⋆

B. Mancillas[1], F. Combes[1,2], and P.-A. Duc[3]

[1] Observatoire de Paris, LERMA, PSL University, CNRS, Sorbonne University, UPMC, Paris, France
[2] Collège de France, 11 Place Marcelin Berthelot, 75005 Paris
[3] Université de Strasbourg, CNRS, Observatoire de Strasbourg, F-67000 Strasbourg, France

Received 2019/ Accepted 2019

ABSTRACT

Shells are fine stellar structures identified by their arc-like shapes present around a galaxy and currently thought to be vestiges of galaxy interactions and/or mergers. The study of their number, geometry, stellar populations and gas content can help to derive the interaction/merger history of a galaxy. Numerical simulations have proposed a mechanism of shell formation through phase wrapping during a radial minor merger. Alternatively, there could be barely a space wrapping, when particles have not made any radial oscillation yet, but are bound by their radial expansion, or produce an edge-brightened feature. These can be distinguished, because they are expected to keep a high radial velocity. While shells are first a stellar phenomenon, HI and CO observations have revealed neutral gas associated with shells. Some of the gas, the most diffuse and dissipative, is expected to be driven quickly to the center if it is travelling on nearly radial orbits. Molecular gas, distributed in dense clumps, is less dissipative, and may be associated to shells, and determine their velocity, too difficult to obtain from stars. We present here a search for molecular gas in nine shell galaxies with the IRAM-30m telescope. Six of them are detected in their galaxy center, and in three galaxies, we clearly detect molecular gas in shells. The derived amount of molecular gas varies from 1.5 10^8 to 3.4 10^9 $M_\odot$ in the shells. For two of them (Arp 10 and NGC 3656), the shells are characteristic of an oblate system. Their velocity is nearly systemic, and we conclude that these shells are phase-wrapped. For the third one (NGC 3934) the shells appear to participate to the rotation, and follow up with higher spatial resolution is required to conclude.

Выборка

Table 1. Properties of the 9 shell galaxies

Name	RA J2000	DEC J2000	cz km s^{-1}	D Mpc	M(HI) log$M_\odot$	L(IR) log$L_\odot$	M(H_2) log$M_\odot$	Ref	Type NED
Arp 230	00:46:24.2	-13:26:32	1720	24.2	9.20	9.49	8.95	(1)	S0pec
NGC 474	01:20:06.7	+03:24:55	2315	32.2	9.63	8.03	<7.7	(2)	SA0
Arp 10	02:18:26.3	+05:39:14	9108	120.	10.2	10.5	-	(3)	S?
NGC 3032	09:52:08.1	+29:14:10	1562	21.2	8.15	9.34	8.42	(4)	SAB0
NGC 3656	11:23:38.6	+53:50:32	2890	42.6	9.27	9.99	9.67	(5)	I0pec
NGC 3934	11:52:12.5	+16:51:05	3779	49.2	9.51	9.98	9.32	(6)	S?
NGC 5018	13:13:01.0	-19:31:05	2816	37.5	8.81	9.54	<7.4	(7)	E3
NGC 7600	23:18:53.8	-07:34:50	3483	39.0	<7.5	–	-	(8)	S0
Arp 295N	23:42:00.8	-03:36:55	6966	93.0	10.2	10.9	10.2	(9)	Sbpec

– References (1) Schiminovich et al. (2013); Ueda et al. (2014) – (2) Rampazzo et al. (2006); Combes et al. (2007); Duc et al. (2015) – (3) Charmandaris & Appleton (1996); Bizyaev et al. (2007) – (4) Combes et al. (2007); Duc et al. (2015) – (5) Balcells et al. (2001); Young (2002) – (6) Bettoni et al. (2011) – (7) Kim et al. (1988); Buson et al. (2004); Ueda et al. (2014) – (8) Turnbull et al. (1999); Cooper et al. (2011) – (9) Hibbard & van Gorkom (1996); Tateuchi et al. (2015) –

Где искали молекулярный газ

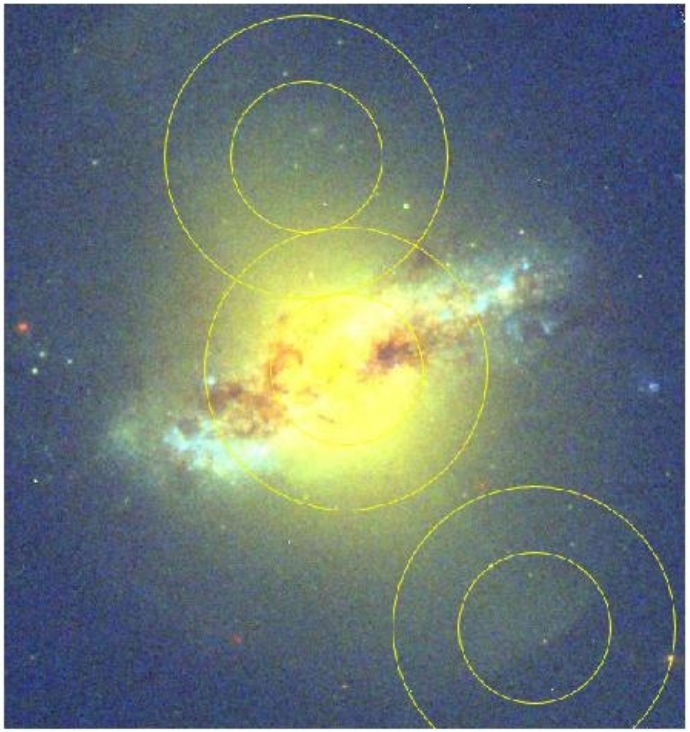

Fig. 1. 23 arcsec (CO(1-0)) and 11 arcsec (CO(2-1)) observed beams towards Arp 230, overlaid on an HST composite image (F336W, F555W, F814W).

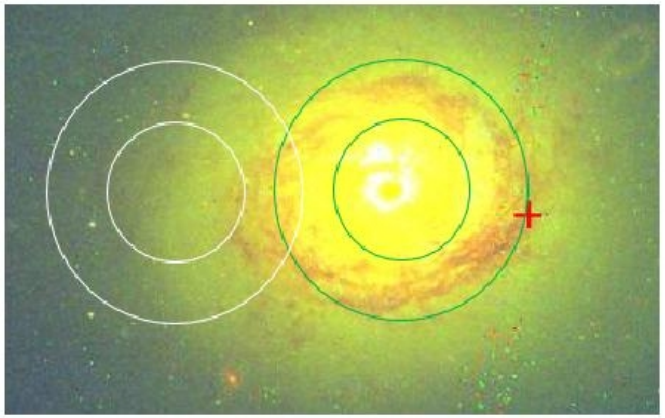

Fig. 5. CO(1-0) and CO(2-1) observed beams on NGC 3032, overlaid on an HST composite image).

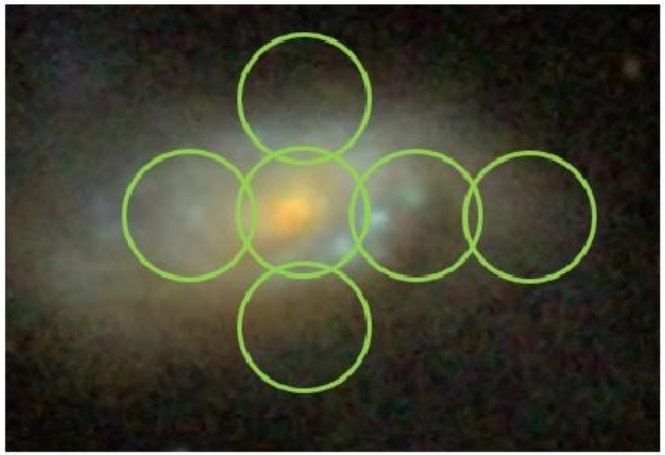

Fig. 8. CO(2-1)- 11 arcsec observed beams in Arp 295N, overlaid on a composite SDSS image.

… даже там, где не ожидалось

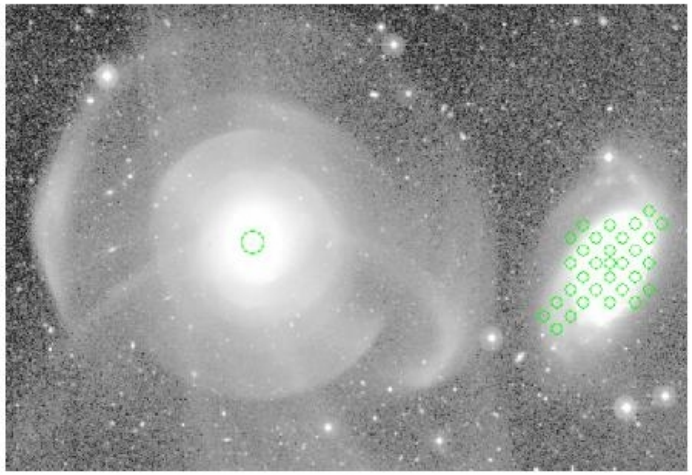

Fig. 2. Image from the CFHT Megacam of NGC 474 and companion NGC 470, enhancing the low surface brighness features, like the shells (Duc et al. 2015). The CO(1-0) beam of 23" is indicated at the center of NGC 474, while the maps of CO(2-1) beams of 11" cover its companion (cf Appendix).

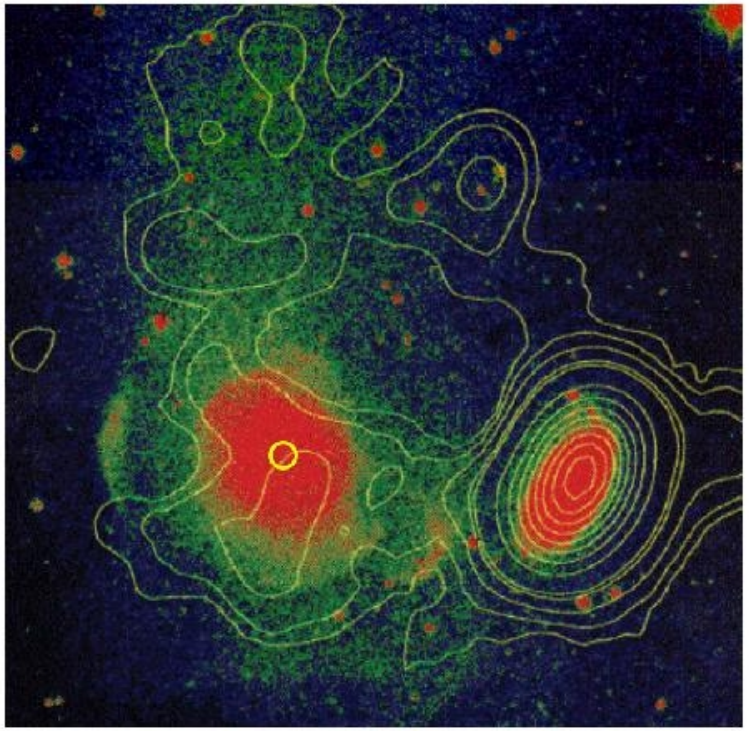

Fig. 3. VLA HI map over Arp 227 (NGC 470 at right and NGC 474 at left), from Schiminovich et al. (1997) and priv. comm. The CO(1-0)-23" beam is indicated with yellow circle.

А вот в этих оболочках нашли

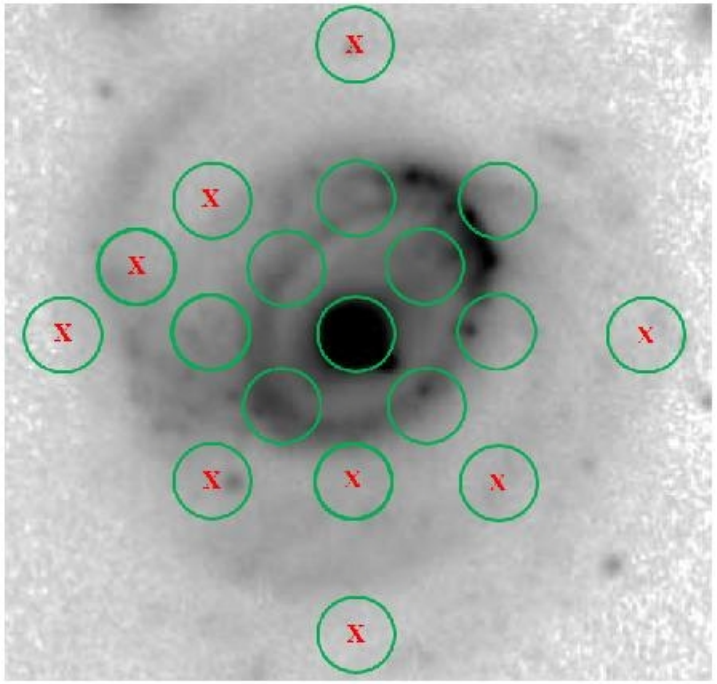

Fig. 4. CO(2-1)- 11 arcsec observed beams in Arp 10, overlaid on the blue optical image, from Bizyaev et al. (2007). The 9 pointings selected to be outside the ring are indicated as a red cross (see Fig. 12)

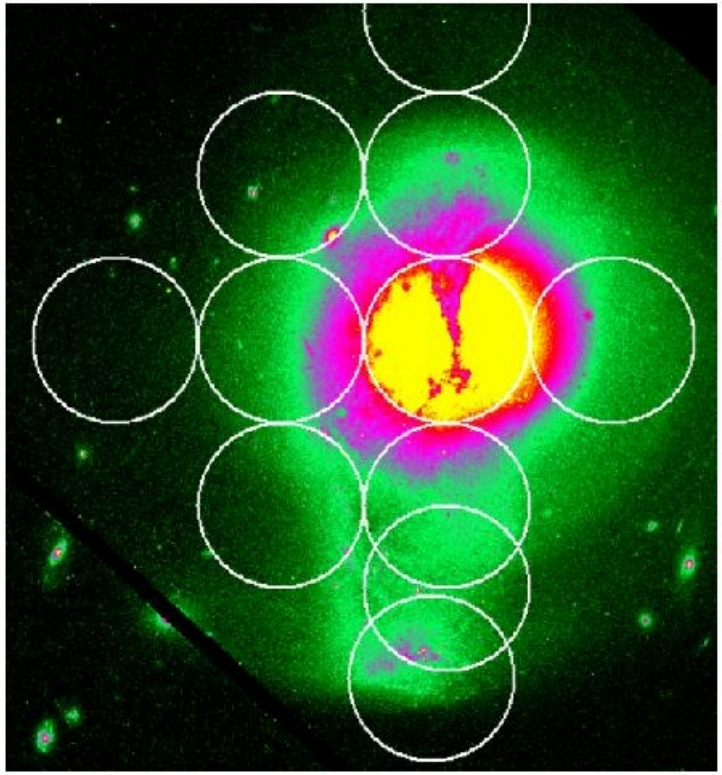

. 6. CO(1-0) observed 23" beams on NGC 3656, superposed on an 6W HST image. Note the prominent N-S dust lane, and the southern ll at the bottom of the image.

и скорости системные!

А в NGC 3934 внешний молекулярный газ вращается

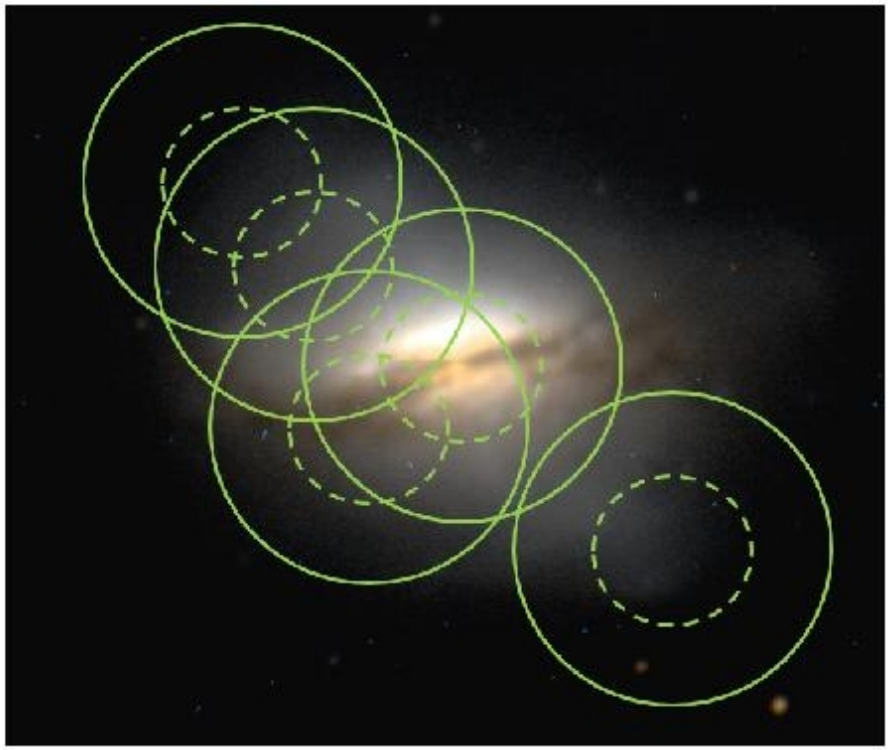

Fig. 7. 23 arcsec and 11 arcsec observed beams in NGC 3934, overlaid on a composite optical image.

Полярное кольцо!?

ArXiv: 1905.12496

LETTER TO THE EDITOR

The Hubble Constant determined through an inverse distance ladder including quasar time delays and Type Ia supernovae

S. Taubenberger[1⋆], S. H. Suyu[1,2,3], E. Komatsu[1], I. Jee[1], S. Birrer[4], V. Bonvin[5], F. Courbin[5], C. E. Rusu[6,7,8], A. J. Shajib[4], and K. C. Wong[9,6]

[1] Max-Planck-Institut für Astrophysik, Karl-Schwarzschild-Str. 1, 85748 Garching, Germany
[2] Physik-Department, Technische Universität München, James-Franck-Str. 1, 85748 Garching, Germany
[3] Institute of Astronomy and Astrophysics, Academia Sinica, 11F of ASMAB, No.1, Section 4, Roosevelt Rd., Taipei 10617, Taiwan
[4] Department of Physics and Astronomy, University of California, Los Angeles, CA 90095-1547, USA
[5] Laboratoire d'Astrophysique, Ecole Polytechnique Fédérale de Lausanne (EPFL), Observatoire de Sauverny, 1290 Versoix, CH
[6] National Astronomical Observatory of Japan, 2-21-1 Osawa, Mitaka, Tokyo 181-8588, Japan
[7] Subaru Telescope, National Astronomical Observatory of Japan, 650 N Aohoku Pl, Hilo, HI 96720
[8] Department of Physics, University of California, Davis, 1 Shields Avenue, Davis, CA 95616, USA
[9] Kavli Institute for the Physics and Mathematics of the Universe (Kavli IPMU, WPI), University of Tokyo, Chiba 277-8583, Japan

Received ...; accepted ...

ABSTRACT

Context. The precise determination of the present-day expansion rate of the Universe, expressed through the Hubble constant H_0, is one of the most pressing challenges in modern cosmology. Assuming flat ΛCDM, H_0 inference at high redshift using cosmic-microwave-background data from Planck disagrees at the 4.4σ level with measurements based on the local distance ladder made up of parallaxes, Cepheids and Type Ia supernovae (SNe Ia), often referred to as "Hubble tension". Independent, cosmological-model-

Результат в цифре

Table 3. Cosmological parameters extracted with MontePython MCMC sampling. Results for different cosmological models are shown for quasar time delays alone (upper four lines) and for the combination of the time-delay measurements with the JLA SN Ia sample (lower six lines). The quoted numbers are the median values, while the uncertainties correspond to the 16th and 84th percentiles.

Cosmological model	Ω_m	Ω_{CDM}	Ω_Λ	Ω_{DE}	Ω_k	w_0	w_a	H_0
Lenses only:								
flat ΛCDM	$0.26^{+0.15}_{-0.14}$	$0.21^{+0.15}_{-0.14}$	$0.74^{+0.14}_{-0.15}$	$\equiv 0$	$\equiv 0$	$\equiv -1$	$\equiv 0$	$72.9^{+2.1}_{-2.3}$
flat wCDM	$0.26^{+0.14}_{-0.14}$	$0.21^{+0.14}_{-0.14}$	$\equiv 0$	$0.74^{+0.14}_{-0.14}$	$\equiv 0$	$-1.74^{+0.60}_{-0.45}$	$\equiv 0$	$80.8^{+5.3}_{-7.1}$
flat w_0w_aCDM	$0.27^{+0.14}_{-0.14}$	$0.22^{+0.14}_{-0.14}$	$\equiv 0$	$0.73^{+0.14}_{-0.14}$	$\equiv 0$	$-1.76^{+0.54}_{-0.44}$	$-0.26^{+1.37}_{-1.21}$	$81.2^{+5.1}_{-6.3}$
non-flat ΛCDM	$0.26^{+0.15}_{-0.14}$	$0.21^{+0.15}_{-0.14}$	$0.72^{+0.16}_{-0.18}$	$\equiv 0$	$0.03^{+0.12}_{-0.15}$	$\equiv -1$	$\equiv 0$	$72.9^{+2.3}_{-2.4}$
Lenses + SNe Ia:								
flat ΛCDM	$0.30^{+0.04}_{-0.03}$	$0.25^{+0.04}_{-0.03}$	$0.70^{+0.03}_{-0.04}$	$\equiv 0$	$\equiv 0$	$\equiv -1$	$\equiv 0$	$73.1^{+2.1}_{-2.2}$
flat wCDM	$0.28^{+0.10}_{-0.11}$	$0.23^{+0.10}_{-0.11}$	$\equiv 0$	$0.72^{+0.11}_{-0.10}$	$\equiv 0$	$-0.96^{+0.21}_{-0.28}$	$\equiv 0$	$72.7^{+3.0}_{-2.9}$
flat w_0w_aCDM	$0.32^{+0.08}_{-0.11}$	$0.27^{+0.08}_{-0.11}$	$\equiv 0$	$0.68^{+0.11}_{-0.08}$	$\equiv 0$	$-0.97^{+0.20}_{-0.29}$	$-0.38^{+1.01}_{-1.08}$	$73.1^{+3.0}_{-3.0}$
non-flat ΛCDM	$0.27^{+0.06}_{-0.05}$	$0.22^{+0.06}_{-0.05}$	$0.66^{+0.08}_{-0.06}$	$\equiv 0$	$0.08^{+0.09}_{-0.13}$	$\equiv -1$	$\equiv 0$	$73.4^{+2.2}_{-2.3}$
non-flat wCDM	$0.27^{+0.09}_{-0.11}$	$0.22^{+0.09}_{-0.11}$	$\equiv 0$	$0.65^{+0.15}_{-0.12}$	$0.08^{+0.09}_{-0.14}$	$-1.02^{+0.24}_{-0.34}$	$\equiv 0$	$73.6^{+3.3}_{-3.3}$
non-flat w_0w_aCDM	$0.30^{+0.08}_{-0.10}$	$0.25^{+0.08}_{-0.10}$	$\equiv 0$	$0.62^{+0.14}_{-0.11}$	$0.09^{+0.08}_{-0.14}$	$-1.05^{+0.25}_{-0.36}$	$-0.29^{+1.02}_{-1.14}$	$74.1^{+3.1}_{-3.3}$

Результат в графике

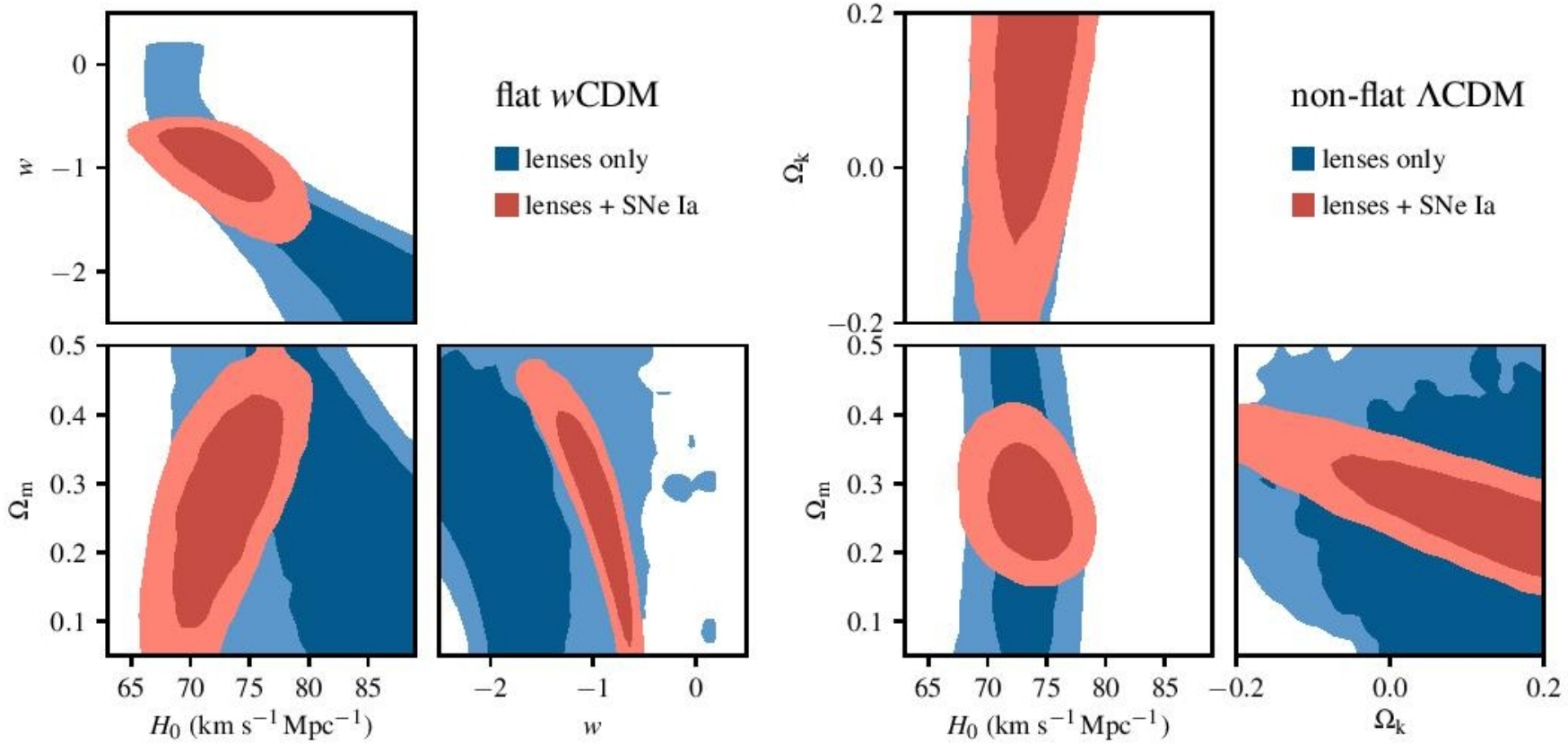

Fig. 1. Contour plots with 68% and 95% confidence regions for H_0, Ω_m, and w in a flat wCDM cosmology (left-hand side), and for H_0, Ω_m, and Ω_k in a non-flat ΛCDM cosmology (right-hand side). Contours based on quasar time delays alone are shown in blue, while those using the inverse distance ladder with strongly-lensed quasars and Type Ia SNe (JLA compilation) are overplotted in red.

И по-любому с Планком не сходится!

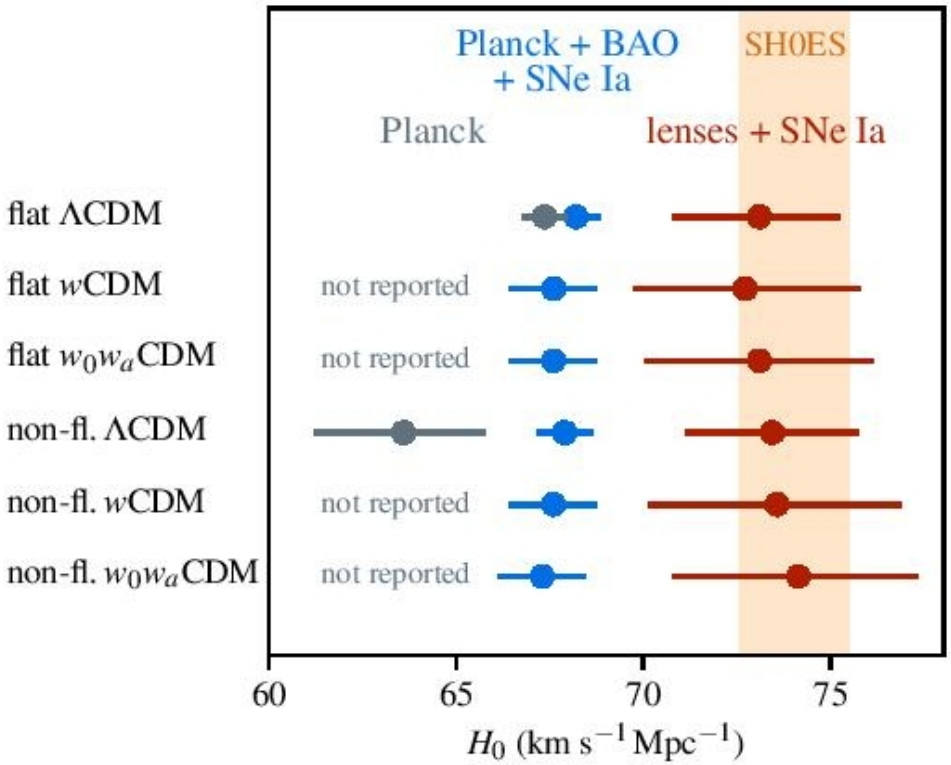

Fig. 3. Comparison between the quasar time delay + SNe Ia inverse distance ladder with other cosmological probes: CMB data from Planck (Planck Collaboration 2018; TT,TE,EE + lowE + lensing), a Planck + BAO + SNe Ia inverse distance ladder from Aubourg et al. (2015), and Cepheid + SN Ia data from the SH0ES project (Riess et al. 2019). The mean and 68% confidence intervals for H_0 are shown for the different probes and different background cosmologies.